

**A NOVEL PATH TO RUNAWAY ELECTRON MITIGATION VIA
DEUTERIUM INJECTION AND CURRENT-DRIVEN KINK
INSTABILITY**

C. PAZ-SOLDAN

Department of Applied Physics and Applied Mathematics, Columbia University
New York, NY 10024, USA. Email: carlos.pazsoldan@columbia.edu

C. REUX, S. SRIDHAR, E. JOFFRIN,
IRFM-CEA/Cadarache,
St. Paul lez Durance, France

Y.Q. LIU, N. EIDIETIS, A. LVOVSKIY, L. BARDOCZI, X. DU
General Atomics
San Diego, CA 92186-5608, USA

S. SILBURN, S. GERASIMOV, F. RIMINI, G. SZEPESEI,
UKAEA/CCFE, Culham Science Centre,
Abingdon, Oxon, OX14 3DB, UK

K. ALEYNIKOVA, P. ALEYNIKOV, V. BANDARU, M. HOELZL, G. PAPP, G. PAUTASSO,
Max-Planck Institute for Plasma Physics,
Greifswald & Garching, Germany

L. BAYLOR, D. SHIRAKI, D. DEL-CASTILLO NEGRETE, D. SPONG
Oak Ridge National Laboratory
Oak Ridge, TN 37831, USA

E. HOLLMANN, Z. POPOVIC, I. BYKOV
Center for Energy Research, University of California San Diego
La Jolla, CA 92093-0417, USA

C. LIU, C. ZHAO, S. JARDIN
Princeton Plasma Physics Laboratory
Princeton, New Jersey 08543-0451, USA

S. JACHMICH, M. LEHNEN,
ITER Organization,
Cadarache Centre, St. Paul lez Durance, France

O. FICKER, E. MACUSOVA,
Institute of Plasma Physics of the CAS,
Prague, Czech Republic

D. CARNEVALE
Dipartimento di Ing. Civile e Ing. Informatica, Universita di Roma Tor Vergata
Rome, Italy

C. SOMMARIVA
Ecole Polytechnique Fed. de Lausanne (EPFL), Swiss Plasma Center (SPC),
Lausanne, Switzerland

A. MANZANARES
Centro de Investigaciones Energeticas, Medioambientales y Tecnologicas,
Madrid, Spain

THE DIII-D TEAM AND JET CONTRIBUTORS*

*See the author list of

E. Joffrin et al. 2019 Nucl. Fusion 59 112021

Abstract

Access to high current density relativistic electron (RE) beams in the DIII-D and JET tokamak reveal excitation of current-driven (low safety factor) kink instabilities that promptly terminate the RE beam on an Alfvénic time-scale, a phenomenon first observed during the early JET carbon wall operation period. Unlike past results however, when combined with the secondary injection of D₂ this phenomenon is found to minimize heating of the first-wall, offering an unexpected alternate pathway to RE mitigation without collisional dissipation. Benign termination is explained by two synergistic effects. First, during large-scale MHD kink events both experiments and MHD orbit-loss modeling support a significant increase in the wetted area of the RE loss. Second, as previously identified at JET and DIII-D, the fast kink loss timescale precludes RE beam regeneration and the resulting dangerous conversion of magnetic to kinetic energy. During the termination the RE kinetic energy is lost to the wall but the current fully transfers to the cold bulk, enabling benign Ohmic dissipation of the magnetic energy on longer timescales. D₂ secondary injection is found to be a necessary ingredient. D₂ injection: 1) facilitates access to low q_a in existing devices (via reduced collisionality & resistivity), 2) directly inhibits RE avalanche by ‘purging’ the high-Z atoms from the RE beam, 3) drives recombination of the background plasma, reducing the density and Alfvén time, and accelerating the MHD growth. Sufficient D₂ purity to achieve benign mitigation is achieved by both shattered pellet secondary injection and conventional massive gas valves. While unexpected, this path scales favorably to fusion-grade tokamaks and offers a novel RE mitigation scenario in principle accessible with the day-one disruption mitigation system (DMS) of ITER.

1. INTRODUCTION AND MOTIVATION

The baseline strategy for mitigating a mature RE beam in ITER is the injection of massive quantities of high-Z atoms (neon or argon) using shattered pellet injection (SPI). This collisional approach is challenged by low rates of high-Z assimilation into the RE beam (slowing collisional damping) as well as the acceleration of the vertical instability. This final effect is predicted to cause the loss of the ITER RE beam to occur at the same I_P regardless of the high-Z quantity assimilated [1]. New approaches to the RE mitigation problem are thus sorely needed.

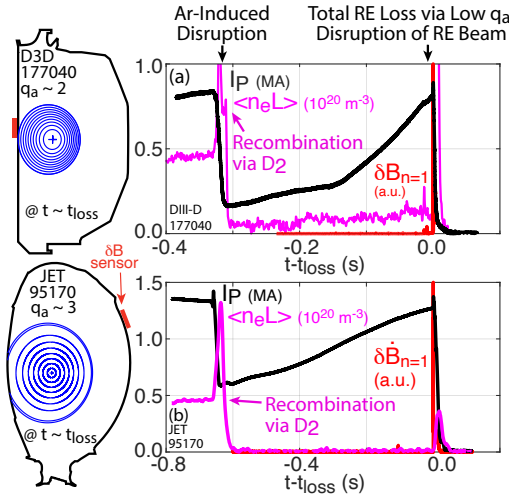


Figure 1: Observation of “D₂+kink” loss events in DIII-D and JET. Access to relatively low q_a in the presence of a recombined plasma state resulting from D₂ injection promotes large-scale MHD instabilities that benignly terminate the RE beam. Examples with flat I_P also exist.

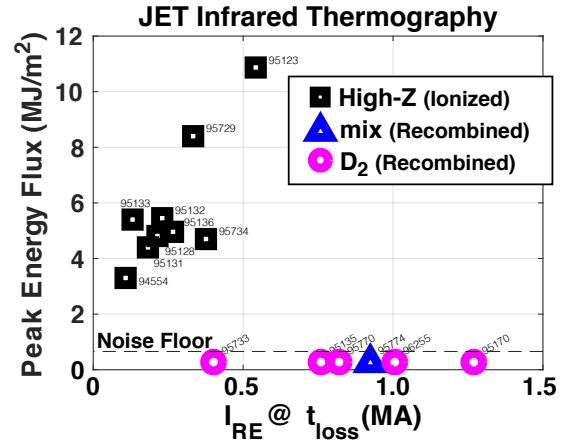


Figure 2: Peak energy flux measurements in JET from infrared (IR) thermography. An increasing trend of energy flux with I_{RE} is found when using high-Z injection, yet dramatically the energy flux is below the noise floor when D₂ injection is used, despite access to far higher I_{RE} being accessed.

Recent observations on DIII-D [2] and JET [3] reveal a promising alternate pathway for mature RE beam mitigation by: 1) injecting D₂ to recombine the background plasma, reducing density (n_e) and decreasing the Alfvén time (τ_A), and 2) exploiting the collisionless plasma state to excite fast current-driven kink instabilities naturally occurring at low safety factor (q_a). DIII-D and JET data in Fig. 1 both show that upon realizing sufficiently high I_P (or sufficiently low q_a), and in the presence of a recombined background plasma, dramatically large MHD events are observed that effectively cause a *second disruption* of the RE beam itself. Even more striking is the absence of first-wall heating observed during these “D₂+kink” termination events, shown in Fig. 2. Even though the RE current (I_{RE}) is greater than RE terminations with high-Z injections (and magnetic energy $E_{mag} \propto I_{RE}^2$ doubly so), the energy flux to the first-wall is found to be below the noise floor for these events. As such, these discharges demonstrate a novel method of mitigating the RE beam. Although the fast kink has been observed before, most notably during early RE beams during JET limiter operation in the 1980s, only in the discharges described in this study has D₂ injection been applied and the synergy with the collisionless background plasma state identified.

This contribution will summarize these findings in terms of the basic benign termination phenomenology (Sec. 2), discuss MHD modeling of the observed phenomenology (Sec. 3), move into discussion of experimental access conditions (Sec. 4), and conclude with an exploration of applying this RE mitigation scheme in ITER (Sec. 5).

2. PHENOMENOLOGY OF THE BENIGN TERMINATION

A detailed description of the phenomenology of the MHD event and the subsequent deconfinement of the RE population is given in Ref. [2], which is here summarized and expanded by inclusion of qualitative IR thermography images. A comparison of a high- I_{RE} , low q_a , recombined loss event is compared to a traditional high q_a , ionized loss event in Fig. 3. In this case, low q_a is accessed by raising I_{RE} , while in later experiments cross-sectional contraction is used to access low q_a at constant or decreasing I_{RE} . Note the interferometer signal ($\langle n_e L \rangle$) reveals the most striking pre-loss indicator of the benign termination: a lack of free-electron density (n_e) indicating a largely recombined background plasma. As discussed in Ref. [4], the recombination effect is thought to be due to the energy loss channel for the input Ohmic power switching from ionization to neutral conduction, facilitated by injection of large quantities of D_2 . As neutral conduction begins to dominate, the bulk temperature (T_e) is lowered below the threshold for ionization, and the plasma recombines. At that point, the remaining free electrons are nearly all relativistic, and the plasma is very collisionless.

The dynamics of the RE final loss (at $t=t_{loss}$) are then totally different. The low q_a case exhibits two discrete HXR bursts indicating strong MHD-driven loss (other discharges have only one), evidenced by a very large $\delta B/B$ of almost 5%. Discrete HXR bursts followed by an absence of HXR emission indicate all REs have been lost. Subsequently, the plasma re-ionizes state, indicating a transfer of the RE current back into bulk thermal current. In contrast, the traditional loss event does not have the large-scale $\delta B/B$, does not have similarly pronounced HXR spikes, and the HXRs persists during the current quench (CQ) phase. As will be discussed, the presence of HXR during the current quench indicates the potential magnetic energy (E_{mag}) transfer into kinetic energy (E_{kin}) in the RE population, which is a damaging phenomenon as $E_{mag} \gg E_{kin}$ [5].

IR camera data (looking opposite the forward-beamed emission) also included in Fig. 3 illustrates the qualitatively different first-wall impact of these two loss scenarios. In the conventional scenario, a localized RE impact is found (complete with carbon dust ejection), followed by persistent wall IR emission, indicating some localized heating occurred. The large $\delta B/B$ loss scenario, in contrast, has a much larger wetted area as evidenced by the broader impact-induced emission, followed by little or no dust, and little or no persistent IR emission. Thus, while qualitative, these images support the basic concept that the large-scale $\delta B/B$ loss events spread the RE E_{kin} over a larger wetted area, which will be later revisited in Sec. 3.

Synchrotron emission (SE) shown in Fig. 4 supports the interpretation that the RE beam can be totally eliminated by the large-scale $\delta B/B$. JET and DIII-D SE data both show a transition from a conventional crescent-shaped SE pattern to no emission at all in the case of JET or a weak residual emission in DIII-D, thought to be visible bremsstrahlung (VB) from the thermal population. This transition occurs over one camera frame, or under one ms, which is the same time-scale of the fast $\delta B/B$ shown earlier. As will be later discussed, SE emission also reveals the potential for loss events that do not drive the loss of the entire RE population. In both DIII-D and JET, a small residual RE beam can be found in cases where the HXR emission is not fully eliminated prior to the CQ, indicating RE beam re-generation arising from the transfer of E_{mag} to E_{kin} . In situations of maximized secondary avalanche gain, JET alone has found the re-emergence of a tiny RE beam. Discussion of avalanche gain is deferred to Sec. 5.

These highlighted discharges are supported by a wider database of JET RE loss events shown in Fig. 5, which

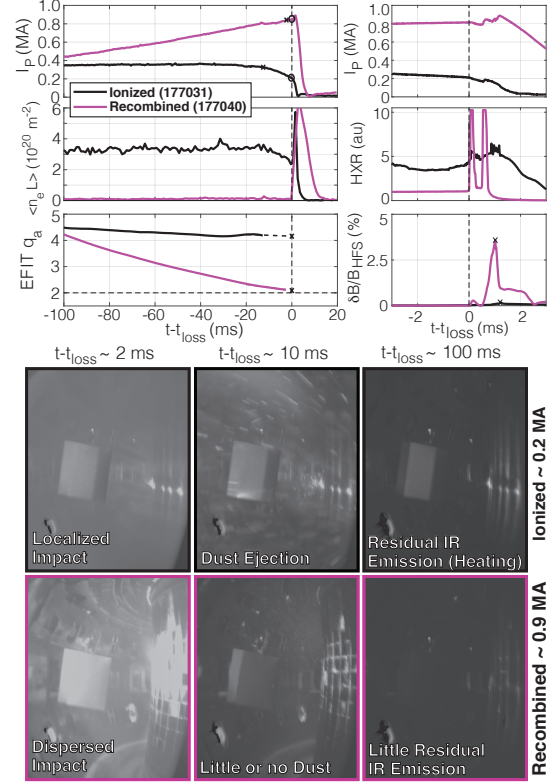


Figure 3: Comparison of conventional and benign RE loss events in DIII-D. The loss event transitions from a gradual process to a singular event with a large $\delta B/B$, a large HXR flash, a large impact wetted area, and an absence of persistent IR emission (heating).

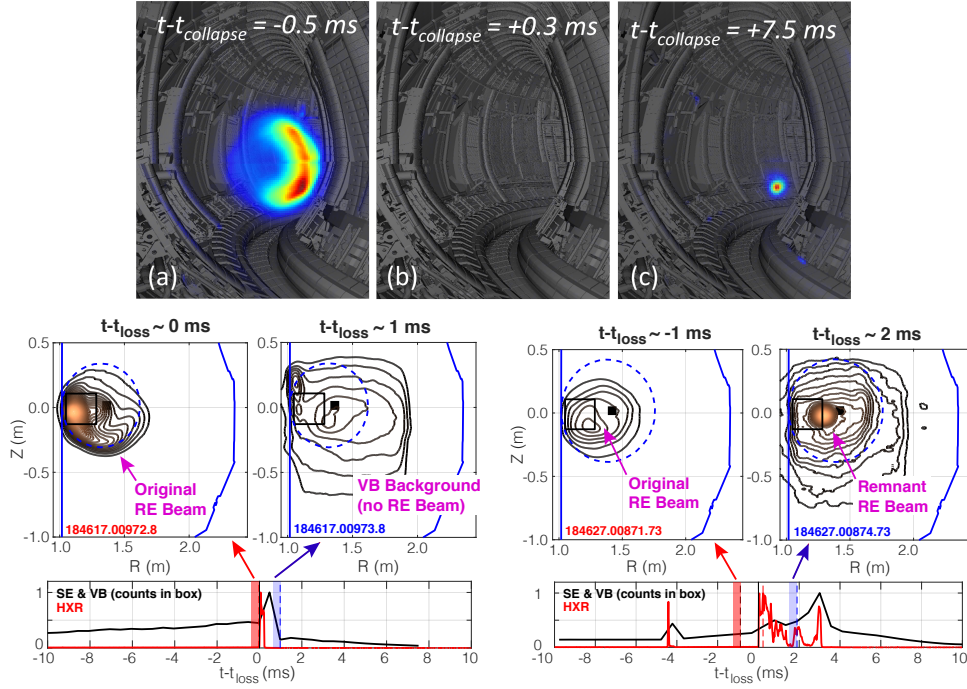


Figure 4: Synchrotron emission in JET and DIII-D, revealing (left) benign cases with complete deconfinement of the RE beam from large-scale $\delta B/B$ event, or (right) non-benign cases with only a partial deconfinement and emergence of a remnant beam.

show that if the D_2 purity is sufficiently high (D_2 being $>95\%$ injected atoms), no E_{mag} to E_{kin} conversion is observed. As such, the larger E_{mag} in these terminations are benignly dissipated as uniform radiation from the now conventional thermal current quench [2]. As was found in Ref. [5], the high-Z cases in contrast are computed to convert a sizeable fraction of E_{mag} into E_{kin} , which then further deposits as localized heating (evidenced by Fig. 2). Interestingly, an intermediate purity regime exists where the outcome can be either benign or non-benign. In JET benign terminations are thus far always found for high purity D_2 injections, however a more complicated picture is found in the DIII-D data. Experimental access to the benign termination will be discussed in Sec. 4.

3. MHD MODELING OF THE BENIGN TERMINATION

MHD modeling of benign termination phenomenology captures the essential features of the MHD loss event. Modeling (JOEKE for JET [8], M3D-C1 for DIII-D [6, 7]) shown in Fig. 6 demonstrates that the near-complete deconfinement of the RE beam, and transfer of the RE current into thermal bulk current is well captured by extended MHD approaches with a fluid treatment of the RE population. Interestingly, the underlying instability is potentially different in JET and DIII-D, with a high q_a double-tearing mode identified at JET [8, 3], yet a conventional low q_a kink instability found in DIII-D [2, 9]. Differences in the expected instability likely arise from differences in the shape of the RE current profile, with broader (or hollow) current profiles naturally expected to exhibit current-driven instability at higher q_a than more peaked profiles. JET current profiles are inferred to be broader (or hollow), consistent with the observation of MHD excitation at higher q_a to be shown in Sec. 4. These findings together demonstrate that the MHD deconfinement effect may be relatively insensitive to the detailed nature of the MHD instability, so long as it grows to sufficient size to deconfine the full RE population and allow the current to transfer to the Ohmic bulk.

Further MHD modeling shown in Fig. 7 of both DIII-D and JET using the MARS-F code [9, 7] recovers the

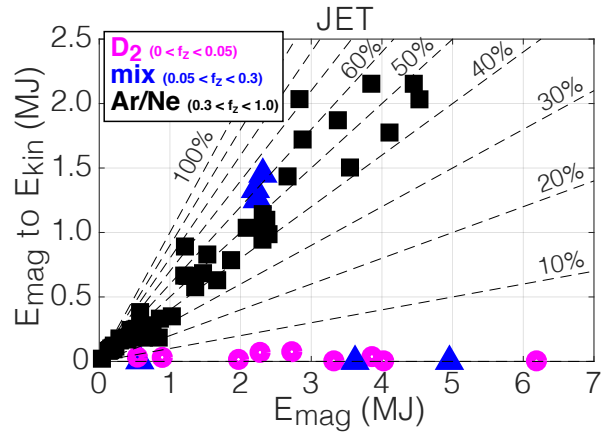


Figure 5: Calculated conversion of E_{mag} to E_{kin} for JET, with the D_2 cases showing very low conversion while the high-Z cases show appreciable conversion. Intermediate mixtures can exhibit both benign and non-benign terminations.

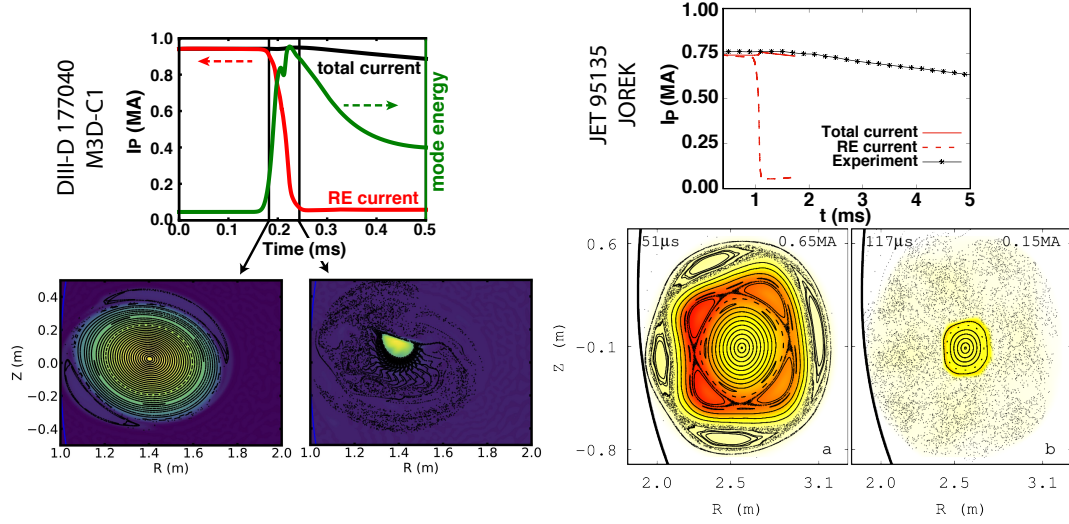


Figure 6: Non-linear extended MHD modeling with a RE fluid model (M3D-C1 for DIII-D [6, 7], JOREK for JET [8]) demonstrate conversion of RE to bulk current after a large-scale MHD event. The DIII-D instability computed is a conventional $q_a=2$ resistive external kink, while the JET instability is found to contain a double-tearing mode due to the hollow current profile.

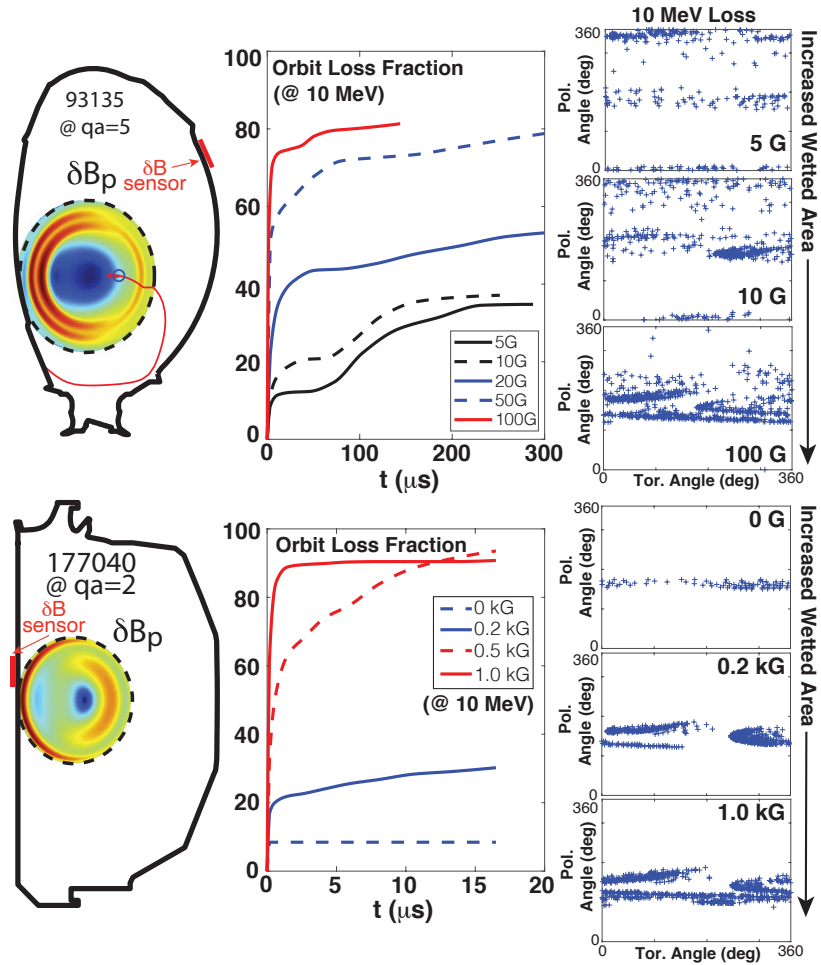


Figure 7: MARS RE-orbit modeling of the expected RE fractional loss for JET and DIII-D. An increasing δB magnitude drives a progressively larger fraction of RE orbits to be lost, and these orbits impact the limiting surface with a progressively larger wetted area. Experimental values for DIII-D are 1 kG, while for JET it is 10 G. Measured δB is highly sensitive to the distance (d) from the plasma to the magnetic sensor (in red), with $\delta B \propto d^{-3}$ computed for these eigenmodes.

increase of the wetted area hypothesized to occur when the RE beam is deconfined by large-scale $\delta B/B$. This modeling proceeds by first calculating the instability mode structure using a linear eigenmode calculation. As the current profiles used for MARS-F modeling in both DIII-D and JET are peaked, conventional low q_a kink modes are found. These magnitude of the linear mode is then arbitrarily scaled, until it approximately matches experiment. For each δB magnitude, the orbits expected for a spatially uniform RE distribution at a given energy and pitch angle (here zero) are calculated, both through the plasma region as well as the vacuum region, until they impact the limiter. Fig. 7 (right) shows that as δB increases, these RE impacts are computed to occur over a progressively larger area. These calculations are somewhat sensitive to the energy and pitch angle of the orbits traced, and so should eventually be convoluted with the expected real and phase space RE distribution function to arrive at a more accurate prediction. The implications of these levels of wetted area for dispersing E_{kin} of RE beams in ITER will be discussed in Sec. 5.

4. EXPERIMENTAL CONDITIONS TO ACCESS THE BENIGN TERMINATION

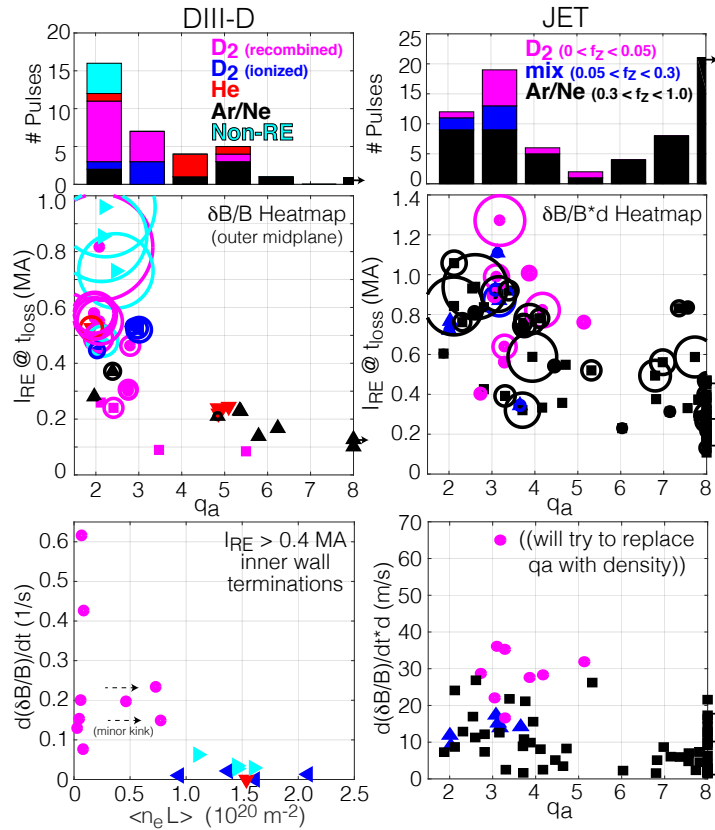


Figure 8: Database comparison of RE loss events for both DIII-D and JET, demonstrating access to low q_a , magnitude of observed $\delta B/B$ and $d(\delta B/B)/dt$ as a function of I_p , q_a , and $\langle n_e L \rangle$.

found to be much less clear, with a wide variance of δB observed even at low q_a and high I_p . The reason for this is unclear, but may be due to sensitivities in the radial δB fall-off, or a wider variety of current profile shapes found in JET (ex, both hollow and peaked profiles) as compared to DIII-D (only peaked profiles). Dedicated scans in DIII-D (not shown) find no dependence on the I_p ramp rate, and find when the current profile is broadened by allowing B_T to fall, higher q_a losses can be promoted. It is also important to note that if the RE beam is position controlled (and high q_a maintained), no loss event is observed regardless of the background plasma state.

Finally, a pseudo-growth rate of the instability ($d(\delta B/B)/dt$) is compared. Here, the findings are clear and consistent for DIII-D and JET. D_2 cases in both exhibit a markedly faster $d(\delta B/B)/dt$, which is especially true if the plasma is fully recombined (low $\langle n_e L \rangle$). This is consistent with an Alfvénic growth, with the fully recombined nature of the equilibrium (low n_e) enabling a particularly fast MHD growth (short τ_A). Particularly interesting in this paradigm are the DIII-D non-RE reference discharges, which access high $\delta B/B$ but not high $d(\delta B/B)/dt$, again supporting the key role of reducing τ_A .

To conclude, experimental access to the benign termination is facilitated by: 1) a recombined plasma state (enabled by D_2 injection), 2) access to low q_a (facilitated by D_2 injection), and 3) high current (facilitated by D_2 injection in existing devices).

DIII-D and JET data demonstrating experimental factors correlated with the benign termination are shown in Fig. 8. The DIII-D database also includes a collection of non-RE (regular) plasma matched disruptions. Consideration is first given to low safety factor access (q_a). This is found to be facilitated by D_2 injection, but significant variation exists. That is, cases without D_2 also can also reach low safety factor, and D_2 cases can also (rarely) undergo a loss event at intermediate q_a (≈ 5). The preponderance of D_2 loss events in both JET and DIII-D however occur at low q_a (2-3 in DIII-D, 3 in JET). Dedicated scans (not shown in this proceedings) demonstrate that for some equally prepared conditions, D_2 beams will access low q_a while high-Z beams trigger the loss event at higher q_a .

Next, the magnitude of the δB is shown as a heatmap against q_a and I_p for both DIII-D and JET. Note that as discussed in Sec. 3, a steep radial fall-off is expected, with $\delta B \propto d^{-3}$, where d is the distance from the magnetic axis to the δB sensor. Nonetheless, we see that in DIII-D a clear trend of increasing $\delta B/B$ is found both as q_a is lowered and I_p rises. The situation in JET is

5. EXTRAPOLATING THE BENIGN TERMINATION TO ITER

This novel RE mitigation path has been demonstrated to be reproducible in DIII-D and JET, and found in JET to result in minimal energy loading onto the first wall [3]. Extrapolation of these findings to ITER requires separate consideration of: 1) the vertically unstable equilibrium evolution, 2) the kinetic energy loading (the large-scale $\delta B/B$ dispersion effect, as shown in Fig. 7), and 3) the conversion of magnetic to kinetic energy (ie, Fig. 5) including the role of secondary generation (avalanche) post-MHD deconfinement. These topics are now treated in turn.

Considering the equilibrium evolution, DINA results shown in Fig. 9 indicate that low q_a rationals are expected to be crossed during the RE beam phase of a high current ITER disruption. Indeed, the crossing of the $q_a = 3$ surface happens due to cross-sectional area contraction during the VDE without much loss of I_{RE} . As such, around 200 MJ of E_{mag} and a several MJ of E_{kin} must be mitigated. Note the exact trajectory expected depends on the radial profile and size of the RE seed, (as well as the effective beam resistivity), as discussed in Ref. [10].

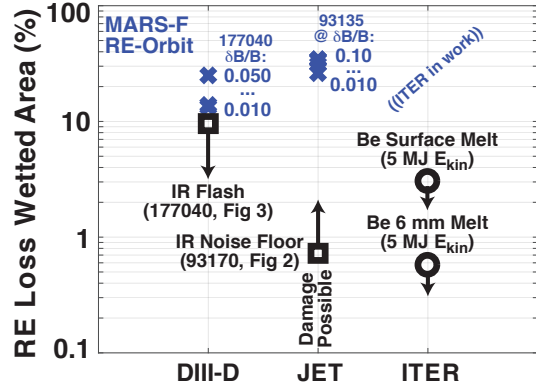


Figure 10: Comparison of RE impact wetted area from: experimental constraints (squares), MARS modeling (\times), and approximate ITER blanket module melt limits (\circ).

rather favorable and consistent across devices. The consistency is not surprising given the self-similar nature of the device geometry and MHD instability across the progression from mid to reactor scale. As such, the excitation of the large-scale $\delta B/B$ is in general rather positive for E_{kin} dispersal across devices. A key open question is whether the large-scale $\delta B/B$ will be realized, and how large it will be. This question was addressed experimentally in Sec. 4. Additional predictive value can be extracted from MHD modeling from JOEKE and M3D-C1, and this work is underway.

Mitigation of the far larger E_{mag} is a more severe challenge. Indeed, the best-case scenario where E_{mag} is dissipated uniformly to the entire first-wall via radiation (100% wetted area) is still a significant energy load to the ITER blanket modules. Worse, the conversion of E_{mag} to E_{kin} commonly results in localized loading, and so is recognized as a key concern [5], particularly so because $E_{mag} \gg E_{kin}$. Fig. 5 showed the favorable result of no conversion from E_{mag} to E_{kin} in JET [3], that was also reported in DIII-D [2]. This is a consequence of: 1) the large-scale $\delta B/B$ promptly deconfining nearly all REs, and 2) the relatively small avalanche gain factor (n_{RE}/n_{seed}) of these devices. While the self-similarity of MHD provides a basis to expect that the large-scale $\delta B/B$ will still expel nearly all REs in ITER, the avalanche gain effect will be completely different from DIII-D and JET to ITER. This is shown in Fig. 11, where the avalanche gain factor is plotted as a function of injection quantity (high-Z and D_2). The beneficial effect of the high-Z ‘purge’ [12, 4] driven by the D_2 injection is clear in both DIII-D and JET, where the Ar expulsion results in a lower expected avalanche gain. Indeed, dedicated scans of the Ar quantity in JET

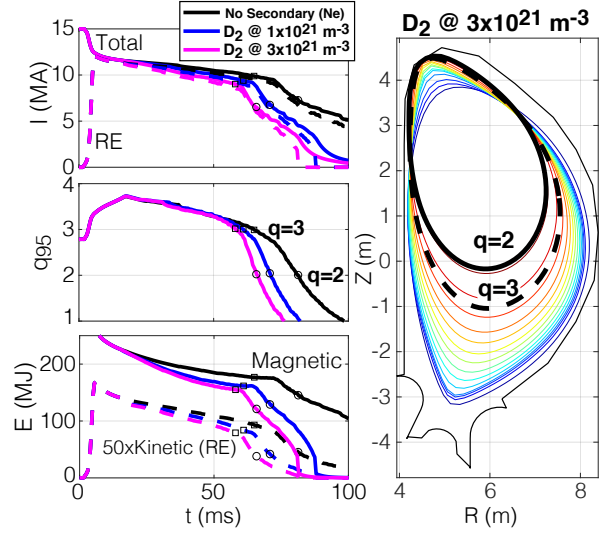


Figure 9: DINA simulations of an ITER post-disruption CQ with a large RE beam, indicating predicted crossing of $q=3$ and 2. Early evolution is dominated by area contraction during the VDE, as opposed to collisional dissipation of the RE beam. The trajectory is relatively insensitive to the D_2 quantity.

While E_{kin} in ITER is far smaller than E_{mag} , it is still a concern due to the commonly observed highly-localized nature of its deposition [11]. As such, dispersal of E_{kin} requires a large wetted area enabled by the large $\delta B/B$ of the excited instability. Figure 10 presents a comparison of experimentally derived limits to the observed wetted area, MARS calculated wetted areas, and ITER expectations for first-wall (Beryllium) melting. The DIII-D upper-bound estimate is taken by assuming the IR flash pattern in Fig. 3 is toroidally symmetric. The JET lower-bound estimate is taken by converting the IR noise floor of Fig. 2 (0.5 MJ/m²) and scaling it to a minimum wetted area to avoid detection for an estimated E_{kin} of 0.5 MJ in JET. ITER estimates are made by taking the per-module blanket energy limits (0.33 MJ for surface melt, 1.75 MJ for 6 mm deep melt) and scaling to the RE E_{kin} . MARS calculations are taken from results shown in Fig. 7. As can be seen, the MARS calculations are actually

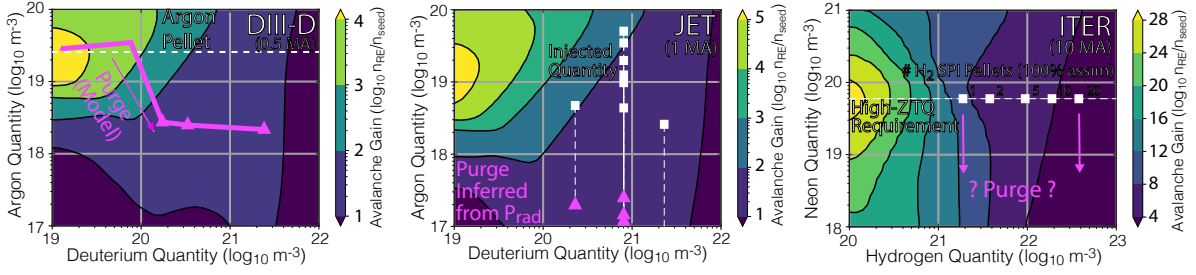


Figure 11: Expected secondary avalanche gain (n_{RE}/n_{seed}) as a function of impurity density for DIII-D, JET, and ITER. For DIII-D, the experimentally injected n_D is shown along with the computed n_{Ar} from modeling [4]. For JET, the experimentally injected n_D is shown along with the n_{Ar} inferred from radiated power magnitude. For ITER, n_H for each SPI pellet is shown.

reveal the re-emergence of a tiny RE beam (pictured in Fig. 4) at the highest Ar quantities and thus the highest avalanche gain factors accessed in JET. This indicates that the fractional RE loss due to the large-scale $\delta B/B$ may be insufficiently complete, though the possible impact of the higher Ar fraction on the MHD loss dynamics itself complicates this picture.

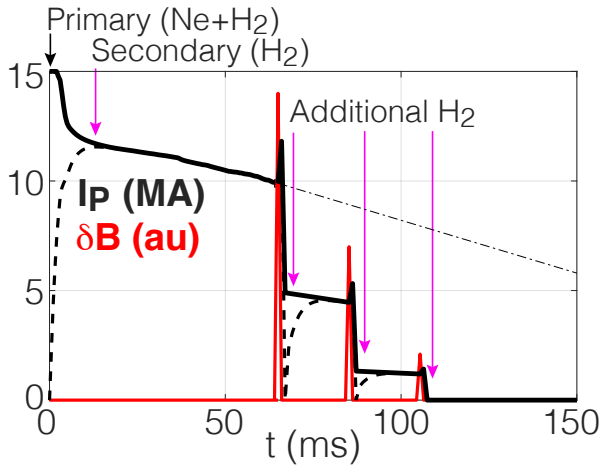


Figure 12: Cartoon scheme of ITER DMS actuation to exploit the D_2 +kink RE mitigation path. The large avalanche gain in ITER will likely require a few cycles of the D_2 +kink loss events. Note ITER plans to use H_2 SPI in place of D_2 in the DMS.

loss event to return to the recombined state. Each loss event should be easily detectable, and could be interlocked to trigger the injection of additional H_2 pellets. Alternatively a pre-programmed train of H_2 pellets could be attempted. These options are technically feasible with the multi-barrel SPI system presently planned as the day-one ITER DMS. This scheme is pictured graphically in Fig. 12, and various elements could be tested in present-day tokamaks and also during the ITER pre-fusion power operation phase.

6. CONCLUSION AND SUMMARY

To conclude, observations on DIII-D and JET reveal a novel benign mitigation scenario for high I_P and E_{mag} RE beams. While further experimentation and modeling is needed, these results open an unexpected and novel pathway for RE mitigation in ITER: inject D_2/H_2 and promote the excitation of large-scale MHD by crossing the kink stability boundary, ideally while in a recombined background plasma state. The large-scale MHD is found in experiment and modeling to increase to RE wetted area, and if the MHD is large enough, completely deconfines the RE population with a non-measurable remnant RE population. Excitation of the large-scale MHD is promoted by D_2 injection, and the largest and fastest $\delta B/B$ is found when the background plasma is recombined. For sufficiently large $\delta B/B$, extended MHD modeling confirms the prompt transfer of the RE current into Ohmic bulk current. Extrapolation of this scheme to ITER requires accounting for the much larger avalanche gain expected, which could drive re-avalanche of even a tiny remnant RE population post-MHD. However, if the initial loss is benign, the scheme can in principle be repeated a few times until the total current can no longer re-avalanche the remnant RE population. Validating the repeatability of access to the “ D_2 +kink” path in situations with high D_2 purity yet large avalanche gain is thus highlighted as a key validation step that cannot be accessed on present-day tokamaks.

ACKNOWLEDGMENTS

Work supported by the US DOE under DE-FC02-04ER54698, DE-SC0020299 and by the ITER Organization (TA C18TD38FU) and carried out within the framework of the EUROfusion Consortium, receiving funding from the Euratom research and training programme 2014-2018 and 2019-2020 under grant agreement No 633053. The views and opinions expressed herein do not necessarily reflect those of the European Commission. DIII-D data shown in this paper can be obtained in digital format by following the links at https://fusion.gat.com/global/D3D_DMP. This work was also supported in part by the Swiss National Science Foundation

DISCLAIMER

This report was prepared as an account of work sponsored by an agency of the United States Government. Neither the United States Government nor any agency thereof, nor any of their employees, makes any warranty, express or implied, or assumes any legal liability or responsibility for the accuracy, completeness, or usefulness of any information, apparatus, product, or process disclosed, or represents that its use would not infringe privately owned rights. Reference herein to any specific commercial product, process, or service by trade name, trademark, manufacturer, or otherwise, does not necessarily constitute or imply its endorsement, recommendation, or favoring by the United States Government or any agency thereof. The views and opinions of authors expressed herein do not necessarily state or reflect those of the United States Government or any agency thereof.

REFERENCES

- [1] KONOVALOV S.V., “Assessment of the runaway electron energy dissipation in ITER”, in *Proc. of 26th IAEA Fusion Energy Conf. (Kyoto, Japan)*, TH/7-1 (2016), URL <https://conferences.iaea.org/indico/event/98/contributions/11966/>
- [2] PAZ-SOLDAN C., EIDIETIS N.W., LIU Y.Q., SHIRAKI D., BOOZER A.H., HOLLMANN E.M., KIM C.C. AND LVOVSKIY A., Kink Instabilities of the Post-Disruption Runaway Electron Beam at Low Safety Factor, *Plasma Physics and Controlled Fusion*, **61**, 054001 (2019), URL <https://doi.org/10.1088/1361-6587/aafd15>
- [3] REUX C., PAZ-SOLDAN C. AND ALEYNIKOV P.B., Demonstration of safe termination of mega-ampere relativistic electron beams in tokamaks, *Physical Review Letters* (in review) (2021)
- [4] HOLLMANN E.M., BYKOV I., EIDIETIS N.W., HERFINDAL J.L., LVOVSKIY A., MOYER R.A., PARKS P.B., PAZ-SOLDAN C., PIGAROV A.Y., RUDAKOV D.L., SHIRAKI D. AND WATKINS J.G., Study of argon expulsion from the post-disruption runaway electron plateau following low-Z massive gas injection in DIII-D, *Physics of Plasmas*, **27**, 042515 (2020), URL <https://doi.org/10.1063/5.0003299>
- [5] LOARTE A., RICCARDO V., MARTIN-SOLIS J.R., PALEY J., HUBER A., LEHNEN M. AND CONTRIBUTORS J.E., Magnetic energy flows during the current quench and termination of disruptions with runaway current plateau formation in JET and implications for ITER, *Nuclear Fusion*, **51**, 73004 (2011), URL <https://doi.org/10.1088/0029-5515/51/7/073004>
- [6] ZHAO C., LIU C., JARDIN S.C. AND FERRARO N.M., Simulation of MHD instabilities with fluid runaway electron model in M3D-C 1, *Nuclear Fusion*, **60** (2020), URL <https://doi.org/10.1088/1741-4326/ab96f4>
- [7] LIU C., ZHAO C., JARDIN S.C., BHATTACHARJEE A., BRENNAN D.P. AND BHATTACHARJEE A., Structure and overstability of resistive modes with runaway electrons Structure and overstability of resistive modes with runaway electrons, *Physics of Plasmas*, **27**, 092507 (2020), URL <https://doi.org/10.1063/5.0018559>
- [8] BANDARU V., HOELZL M., REUX C., FICKER O., SILBURN S., LEHNEN M., EIDIETIS N. AND TEAM J., Magnetohydrodynamic simulations of runaway electron beam termination in JET, *Plasma Physics and Controlled Fusion*, **63**, 035024 (2021), URL <https://doi.org/10.1088/1361-6587/abdbcf>
- [9] LIU Y., PARKS P., PAZ-SOLDAN C., KIM C. AND LAO L., MARS-F modeling of post-disruption runaway beam loss by magnetohydrodynamic instabilities in DIII-D, *Nuclear Fusion*, **59**, 126021 (2019), URL <https://doi.org/10.1088/1741-4326/ab3f87>
- [10] ALEYNIKOVA K., HUIJSMANS G.T.A. AND ALEYNIKOV P.B., Linear MHD stability analysis of post-disruption plasmas in ITER, *Plasma Physics Reports*, **42**, 486 (2016), URL <http://link.springer.com/10.1134/S1063780X16050019>
- [11] REUX C., PLYUSNIN V.V., ALPER B., ALVES D., BAZYLEV B. AND BELONOHY E., Runaway electron beam generation and mitigation during disruptions at JET-ILW, *Nuclear Fusion*, **55**, 093013 (2015), URL <https://doi.org/10.1088/0029-5515/55/9/093013>
- [12] SHIRAKI D., COMMAUX N., BAYLOR L.R., COOPER C.M., EIDIETIS N.W., HOLLMANN E.M., PAZ-SOLDAN C., COMBS S.K. AND MEITNER S.J., Dissipation of post-disruption runaway electron plateaus by shattered pellet injection in DIII-D, *Nuclear Fusion*, **58**, 056006 (2018), URL <https://doi.org/10.1088/1741-4326/aab0d6>